The Role of Metal Disulfide Interlayer in Li-S Batteries

Andrea Paolella[a,1], Dharminder Laul[a,b,1], Vladimir Timoshevskii[a], Wen Zhu[c], Sergio Marras[d], Giovanni Bertoni[e], Alexander Sean Wahba[f], Gabriel Girard[a], Catherine Gagnon[a], Lisa Rodrigue[c], Basile Commarieu[a], Abdelbast Guerfi[a], Raynald Gauvin[b], Michel L.Trudeau[c], Ashok Vjih[c], Michel Armand[g] and Karim Zaghib[a,*]

[a] Centre d'excellence en électrification des transports et stockage d'énergie, Hydro-Québec Innovation, 1800, boul. Lionel-Boulet, Varennes QC, Canada J3X 1S1

[b] McGill University, Department of Mining and Materials Engineering, 3610 Rue University, Montréal, Québec, H3A 0C5, Canada

[c] Material Science, Institute de Recherche de Hydro- Québec, 1800, boul. Lionel-Boulet, Varennes QC, Canada J3X 1S1

[d] Nanochemistry Department, Istituto Italiano di Tecnologia, via Morego 30, 16130 Genova, Italy

[e] IMEM-CNR, Parco Area delle Scienze 37/A, 43124 Parma, Italy

[f] McGill University, Department of Chemistry, 801 Sherbrooke St. West, Montréal, Québec H3A 0B8, Canada

[g] CIC energigune, Parque Tecnologico, C/Albert Einstein 48, CP 01510 Minano, (Alava) Spain

[1] The authors equally contributed to this work

* Corresponding author: Zaghib.Karim@ireq.ca

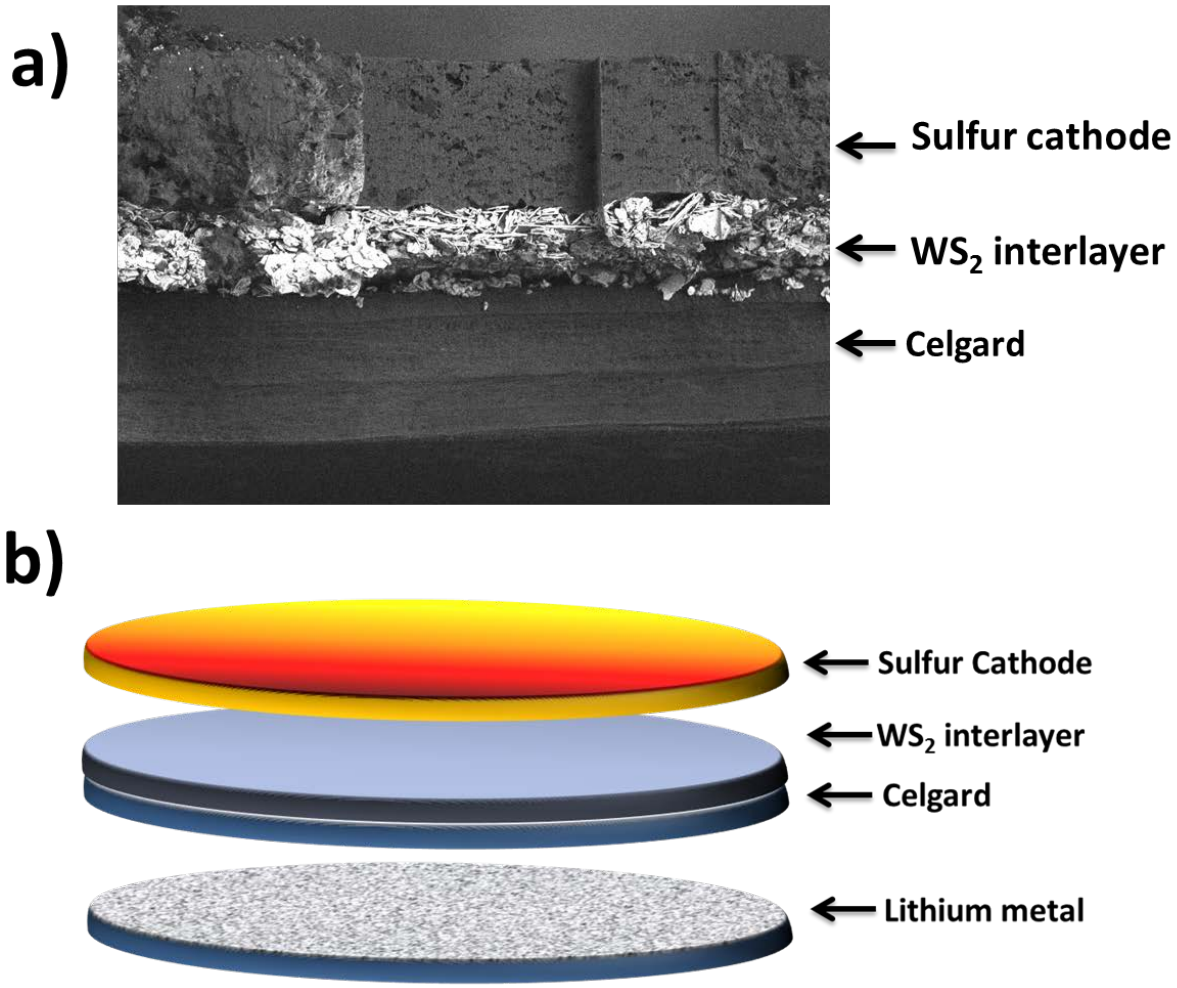

Figure S1: *a) SEM image of Celgard with WS2 interlayer and Sulfur cathode after cycling and b) schematic of battery cycling*

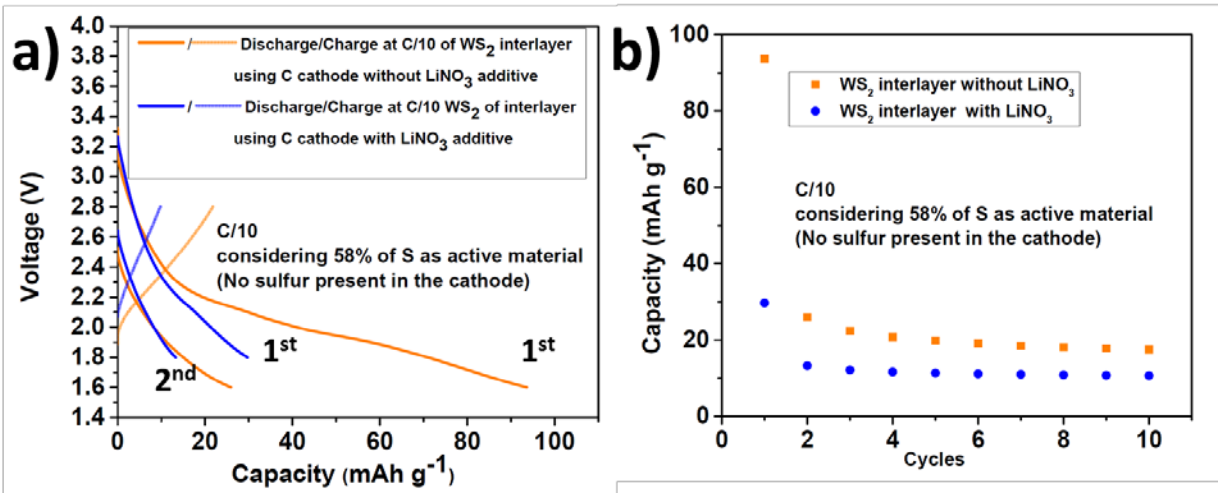

Figure S2: *a) discharge/charge curves and b) capacity trend during cycles of carbon cathode and WS_2 interlayer. The batteries were cycled at C/10 considering the theoretical capacity of sulfur to set the current.*

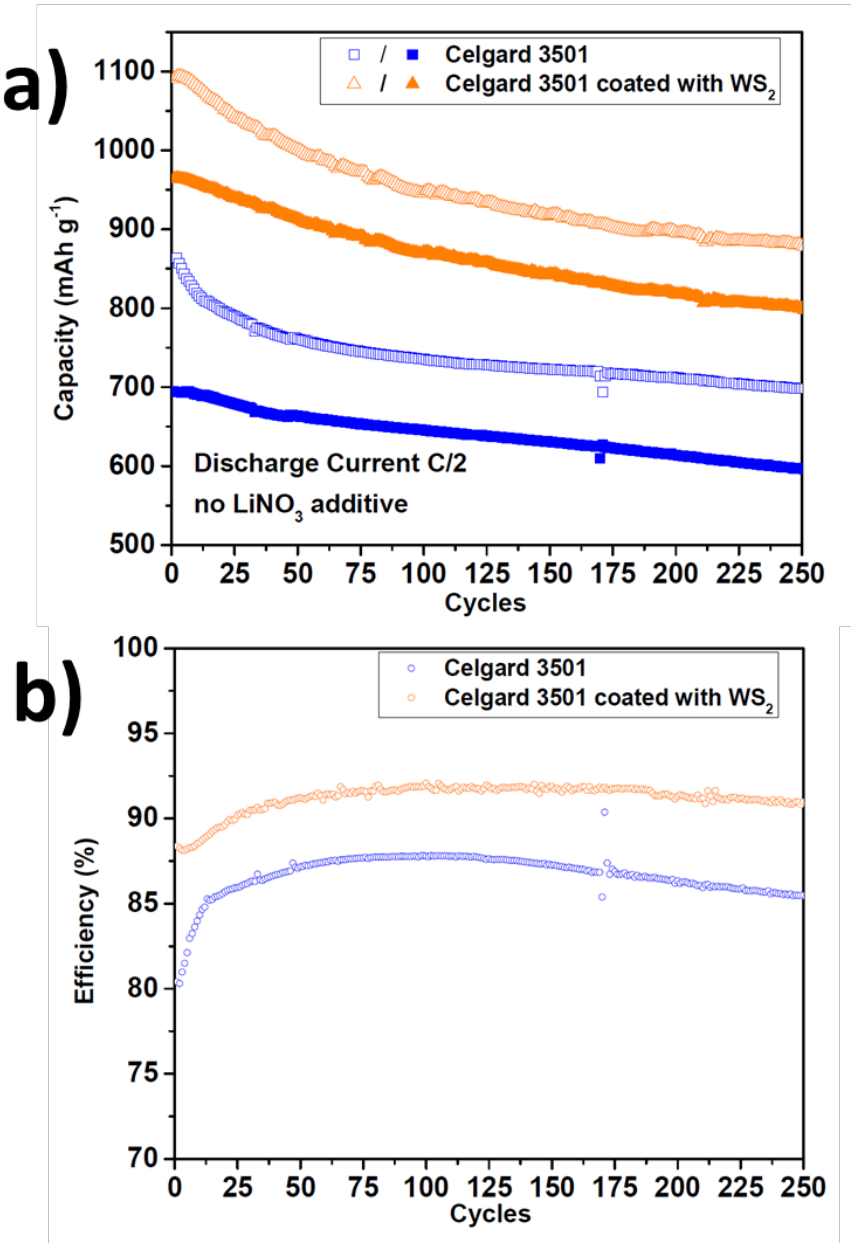

Figure S3: *a) charge/discharge curves of batteries using standard Celgard and Celgard coated with WS_2, b) efficiency profile of the two different separators*

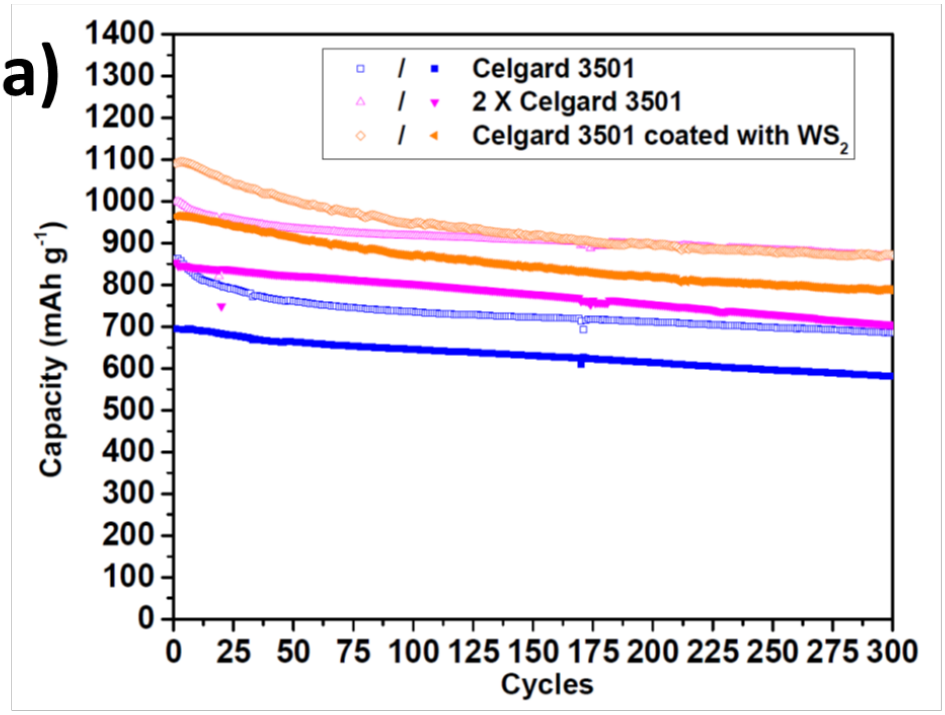

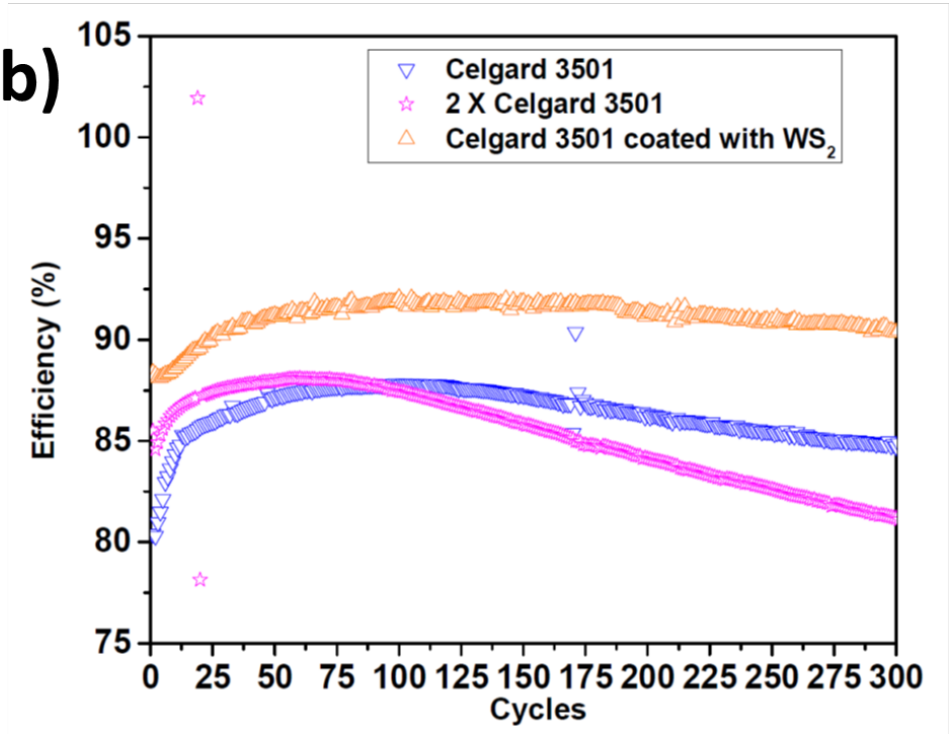

Figure S4: *Discharge plot at C/2 comparing standard Celgard 3501, double Celgard and Celgard coated by WS_2*

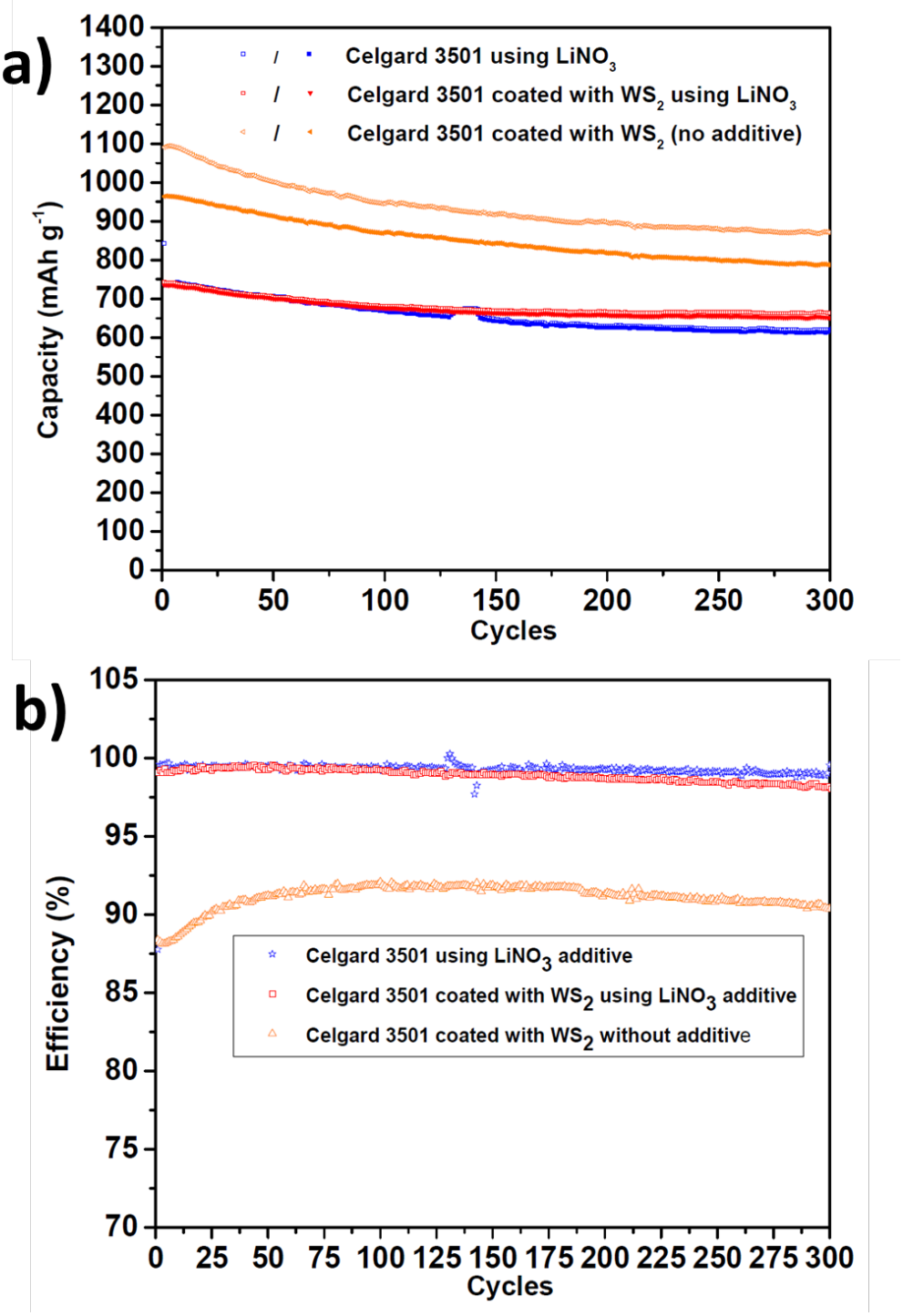

Figure S5: *a) charge/discharge curves related to standard Celgard coated with WS_2 with and without $LiNO_3$ additive, b) efficiency profile of the two different electrolyte conditions*

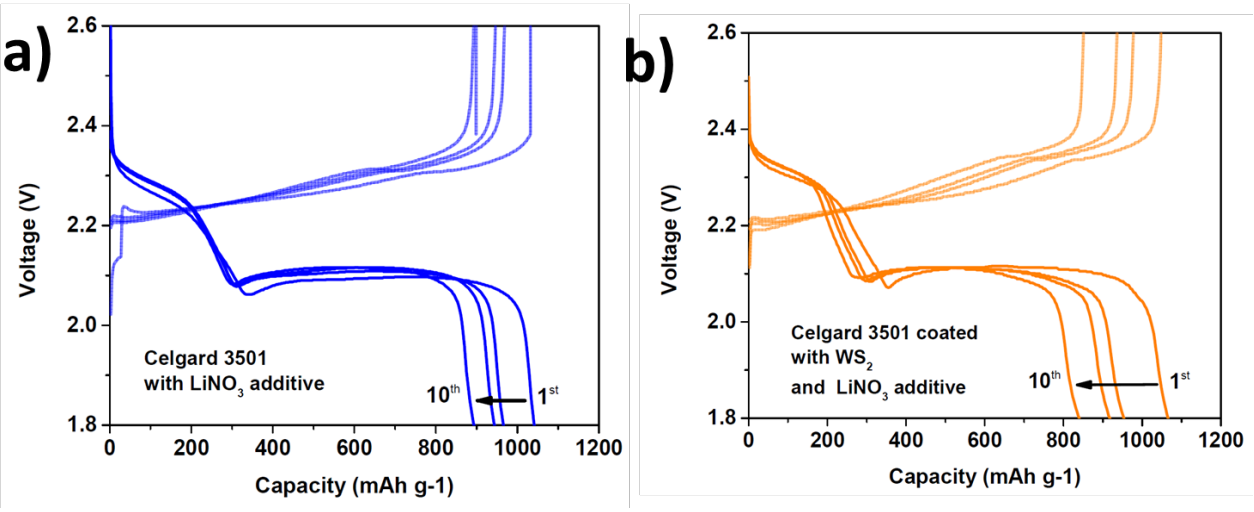

Figure S6: *discharge capacity comparison of standard and WS_2 coated Celgard at a) C/10 and b) C/2 using $LiNO_3$ additive*

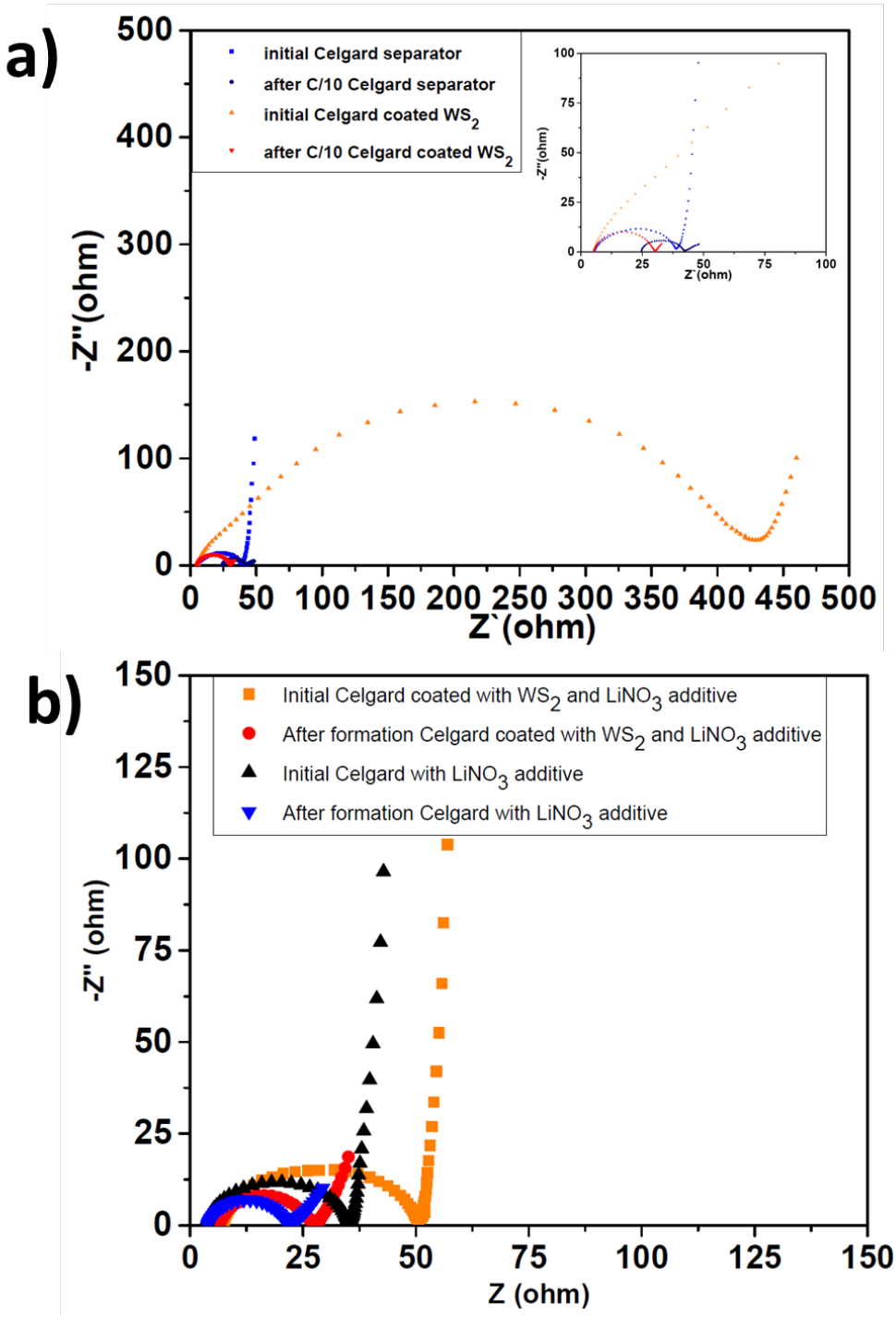

Figure S7: *a) Nyquist plots for standard Celgard and Celgard coated with WS_2 without using $LiNO_3$ and b) Nyquist plots for standard Celgard and Celgard coated with WS_2 using $LiNO_3$*

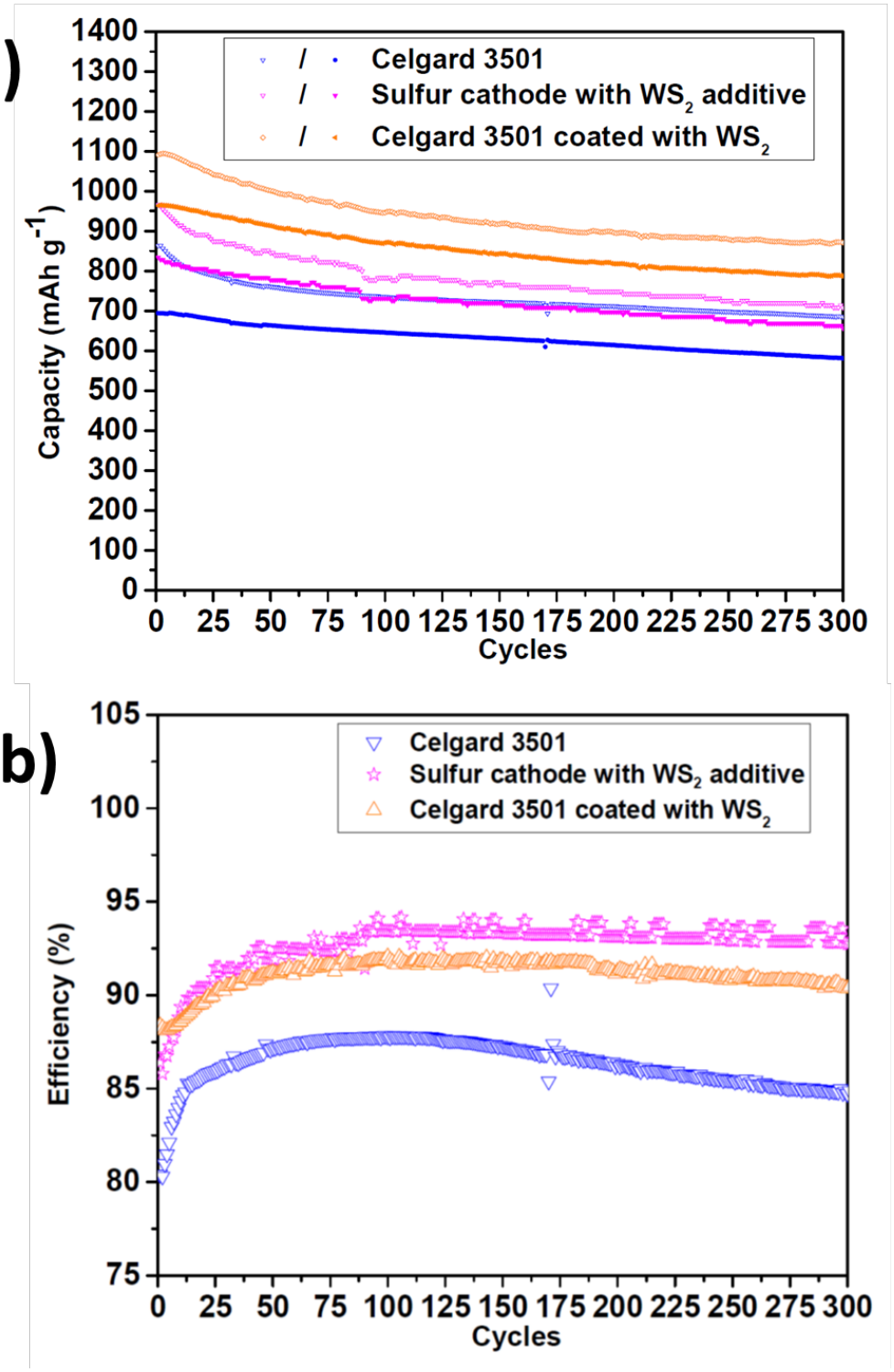

Figure S8: *discharge curves at C/2 comparing standard Celgard 3501 separator, sulfur cathode with WS_2 as additive and Celgard 3501 coated with WS_2*

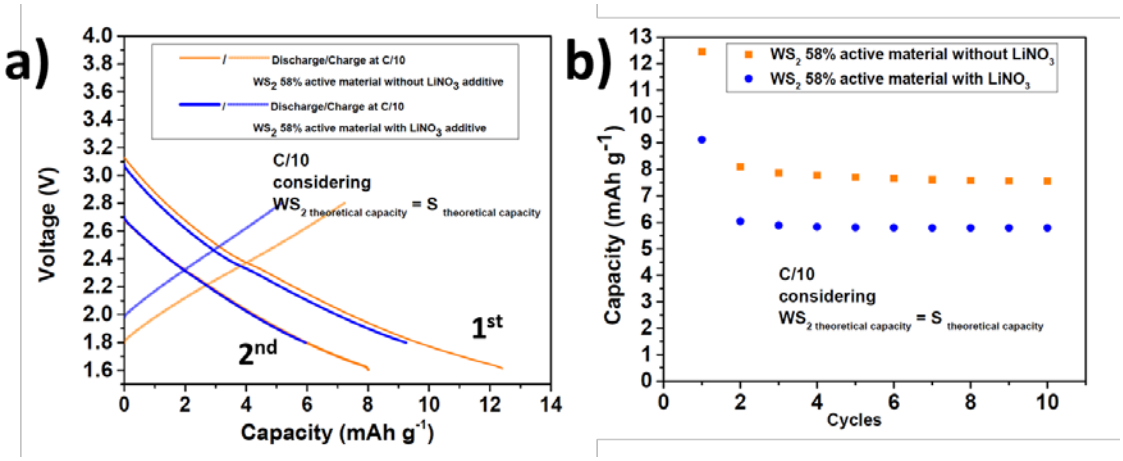

Figure S9*: a) discharge/charge curves and b) capacity trend during cycles of cathode containing 58% of WS2. The batteries were cycled at C/10 considering the theoretical capacity of sulfur to set the current.*

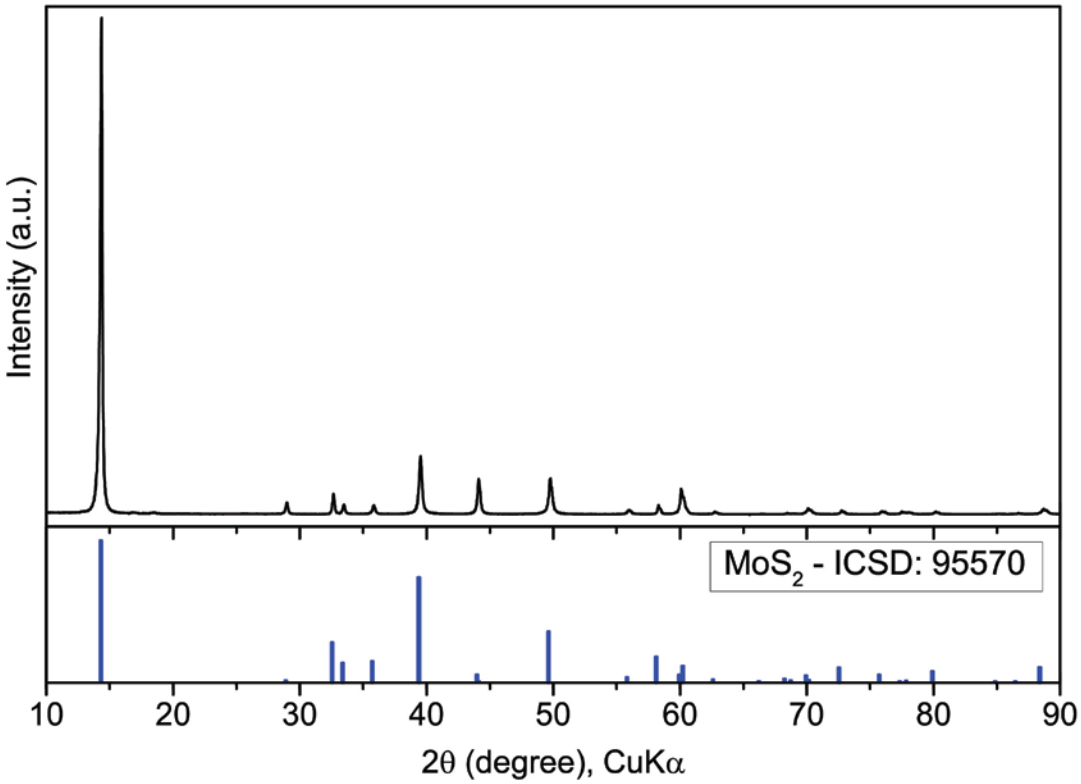

Figure S10: *XRD pattern of Celgard coated with MoS_2*

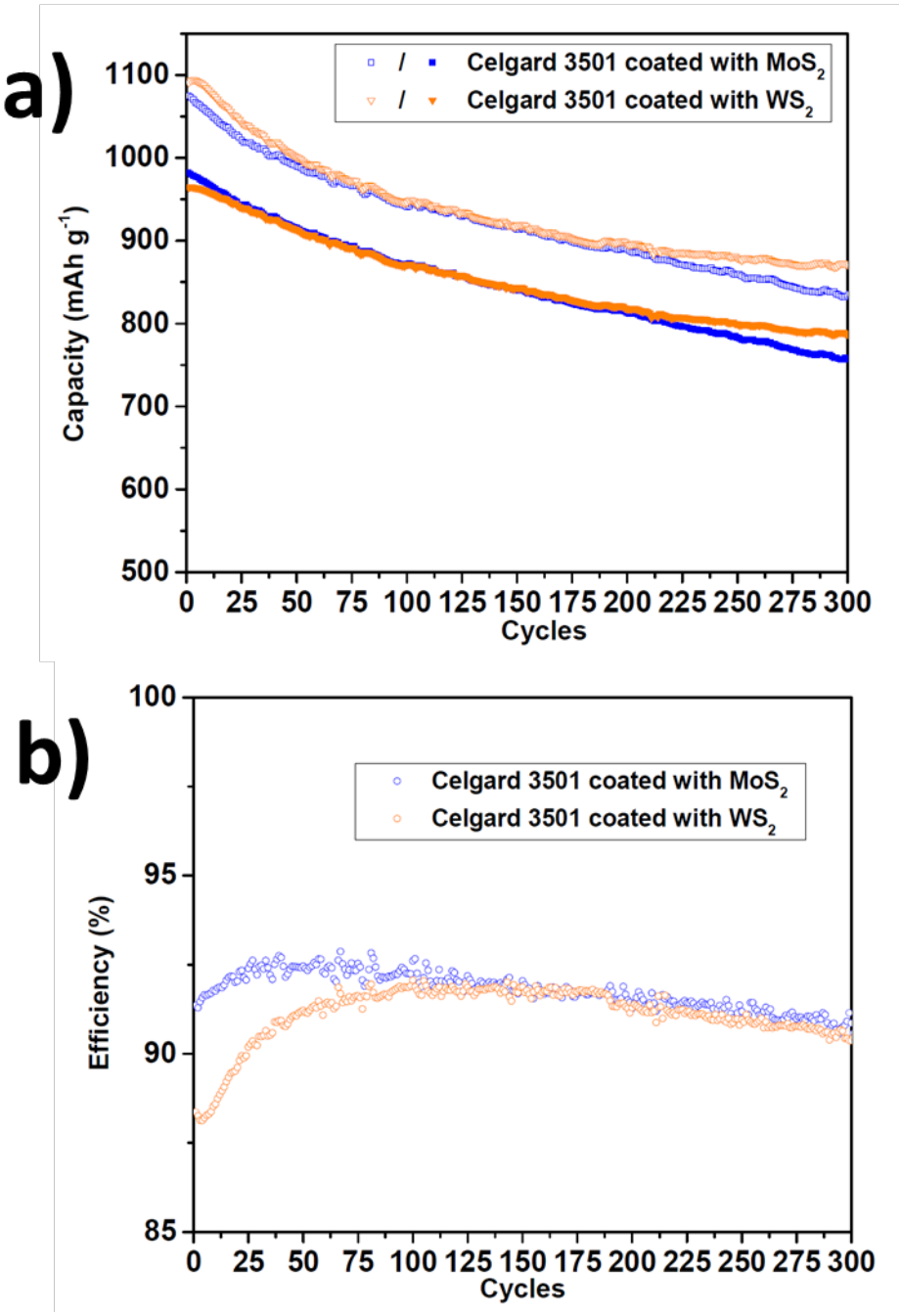

Figure S11: charge/ *discharge curves comparing Celgard 3501 coated with WS_2 and MoS_2*

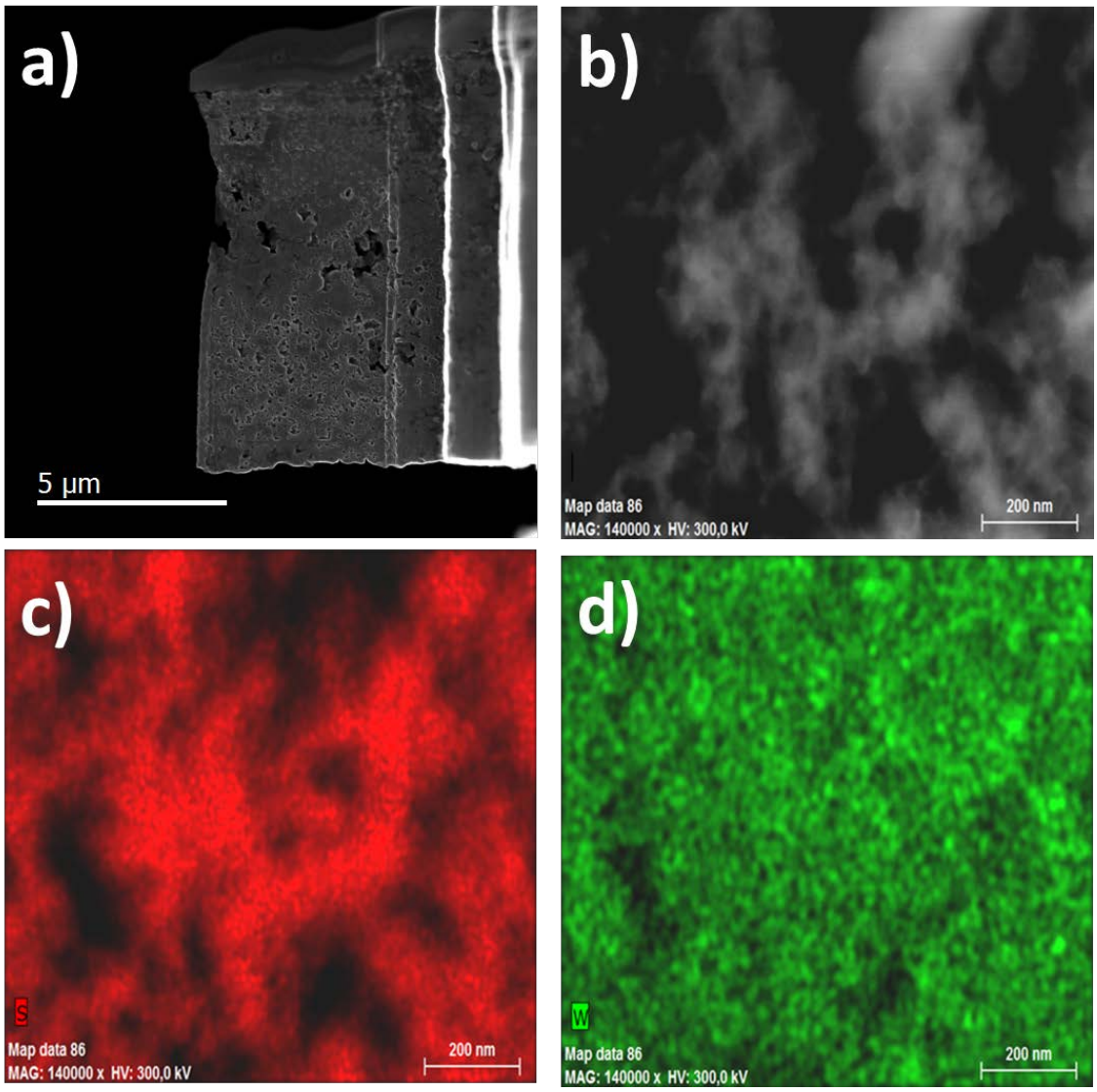

Figure S12: *a) STEM image of the cycled cathode with WS_2 interlayer and $LiNO_3$, b-d) STEM image and EDS mapping showing the presence of tungsten in the cathode*

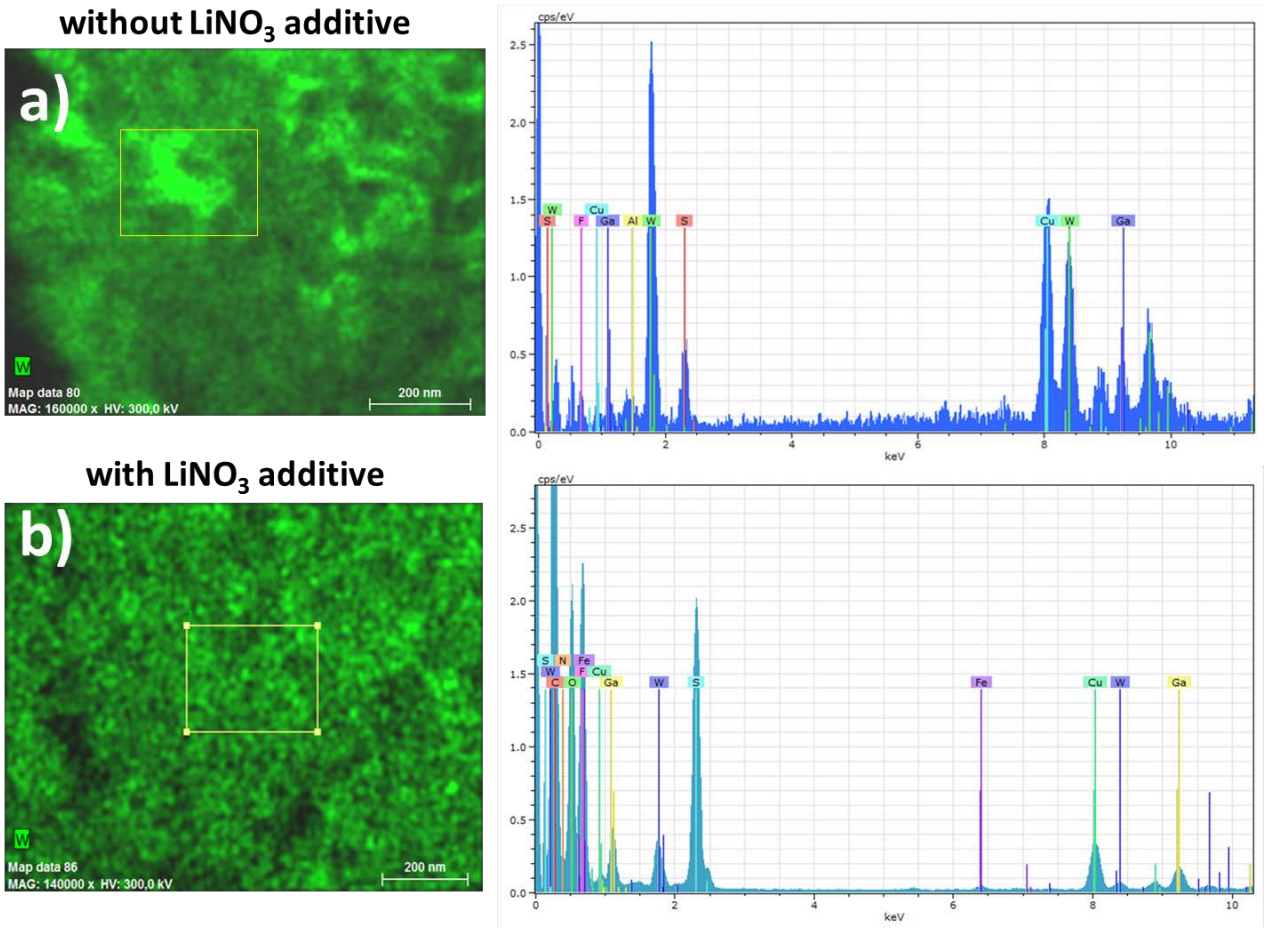

Figure S13: *W EDS mapping of the cycled cathode with WS_2 interlayer a) without $LiNO_3$ additive and b) with $LiNO_3$ additive. The presence of Ga is due to FIB. Cu is related to the grid. Fe is related to the pole piece of the microscope. Al comes from the sample holder. C, N, F, O come from the cathode.*

a)

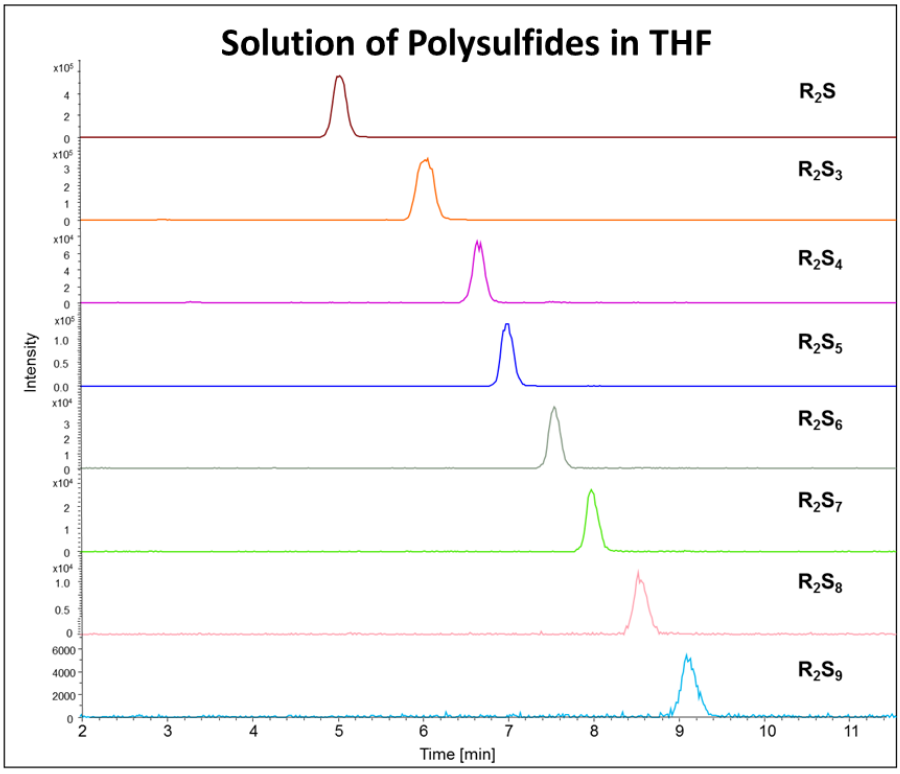

b)

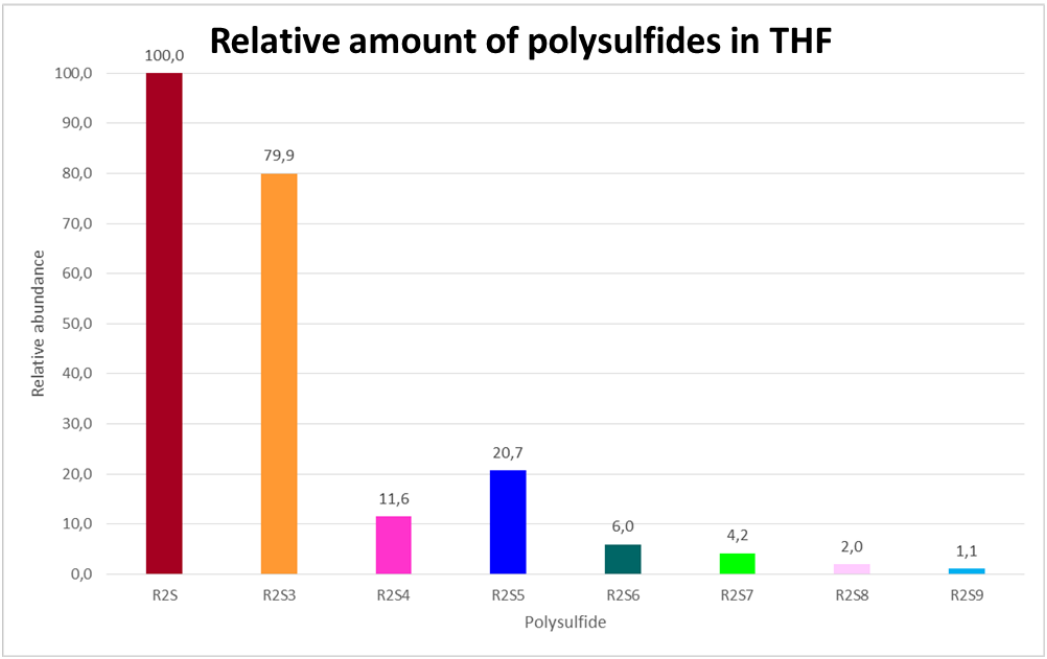

Figure S14: ***a)*** *HPLC-MS analysis of polysulfide THF solution and b) their relative amount distribution*

a)

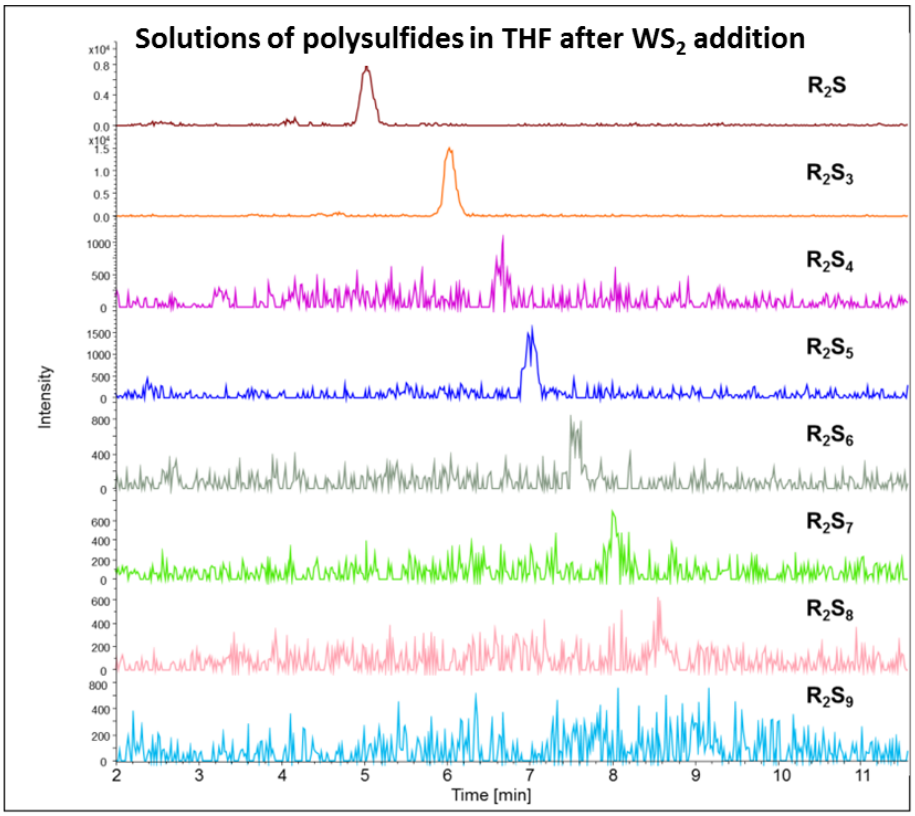

b)

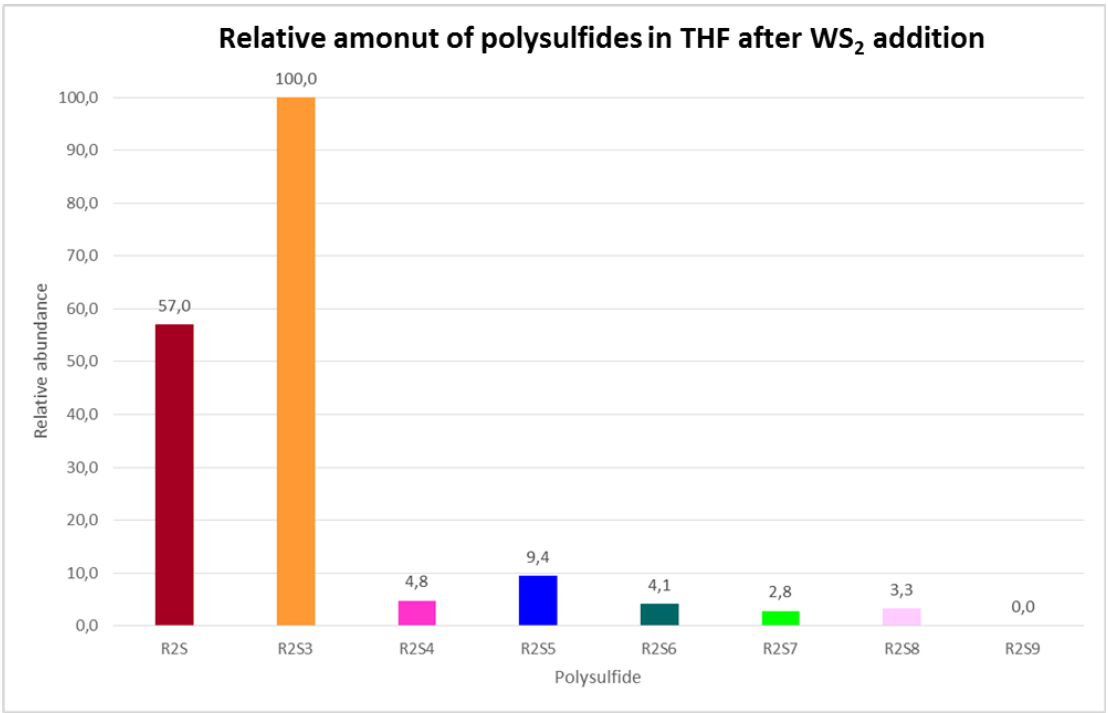

Figure S15: ***a)*** *HPLC-MS analysis of polysulfide THF solution after WS_2 addition and b) their relative amount distribution*

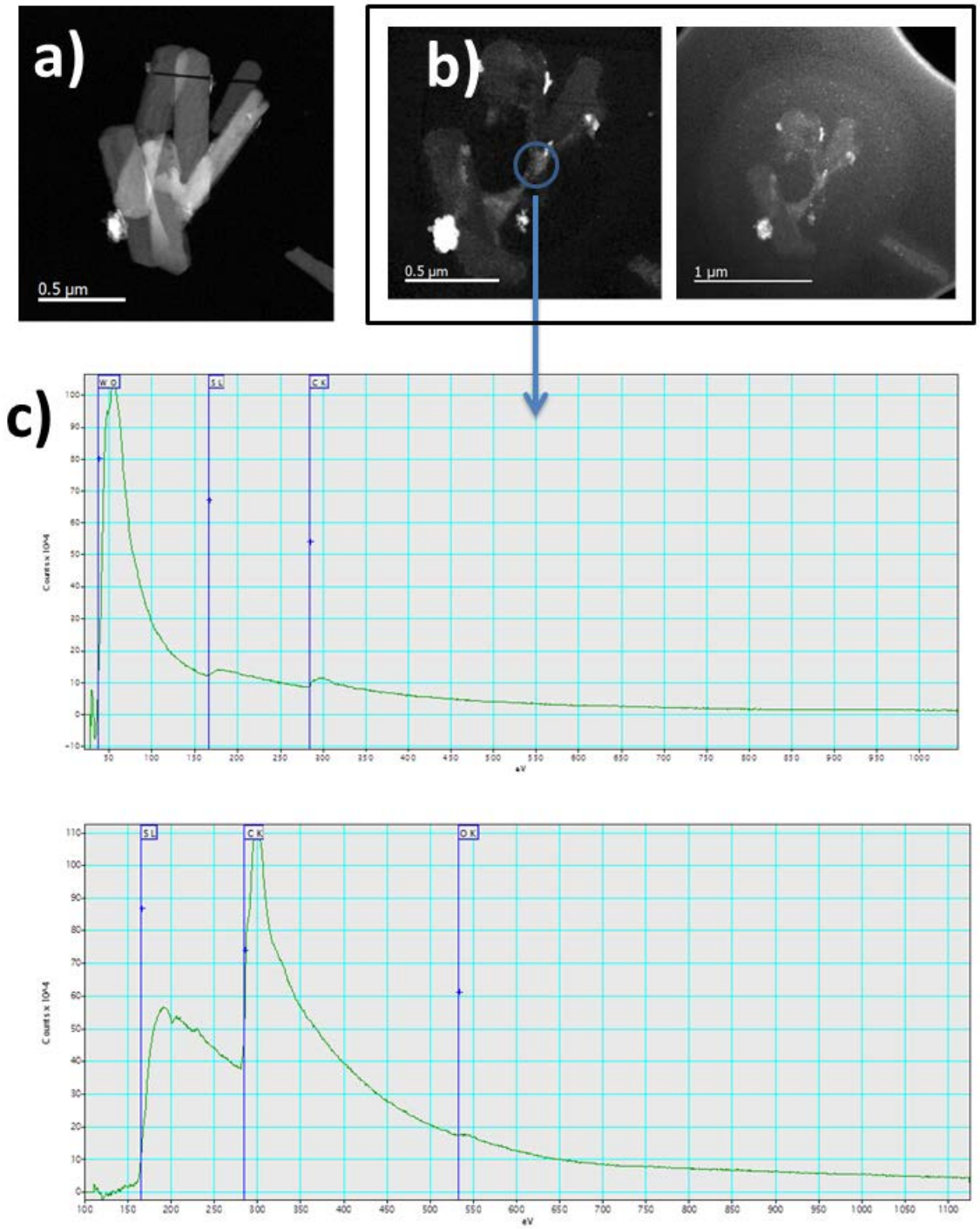

Figure S16: *a) HAADF-STEM image and (b) DF-TEM images of the supernatant after addition of WS_2 in polysulfide THF solution after evaporation of the THF solution, and c) EELS spectra*

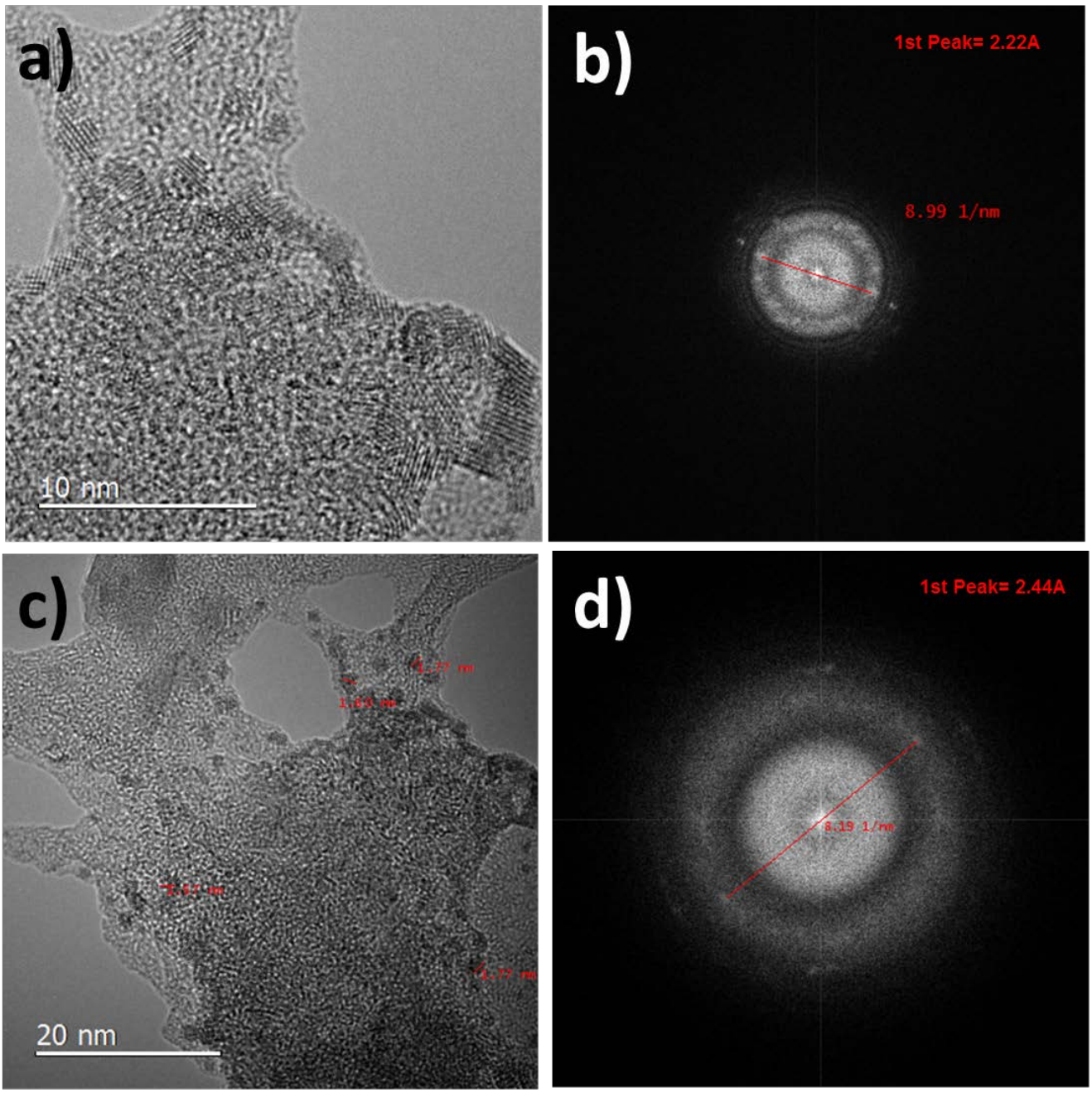

Figure S17: *a–c) TEM images and b-d) diffraction patterns of the nanoparticles observed in the supernatant after evaporation of the THF solution.*

Computational details

We used Quantum-Espresso DFT program package[1] with projector augmented-wave (PAW) pseudopotentials. The PAW datasets were downloaded from THEOS pseudopotential database (http://materialscloud.org/sssp) of École Polytechnique Fédérale de Lausanne. We used the energy cutoffs of 70Ry and 400Ry for wavefunction and electronic density expansions respectively in all our calculations. These convergence parameters as well as PAW datasets were thoroughly tested for correct reproducing of both structural and energetic parameters of WS_2 structure. The calculated in-plane lattice parameter of WS2 monolayer was 3.19 Å, which is in excellent agreement with previously calculated theoretical value[2] (3.18 Å), as well as with experimental data[3] (3.15 Å). To make sure that our computational scheme can correctly reproduce the binding energy of W atom, we calculated this value for a WS_2 monolayer within a 4x4 supercell. The resulting binding energy of 6.99 eV (relative to bulk W chemical potential) matched well the one (6.98 eV) we obtained for exactly the same setup with an all-electron LAPW code[4].. All calculations were performed in a *spin-polarized* approximation. To calculate the binding energies of a single W atom in the WS_2 sheet/ribbon, both two-dimensional monolayer and nanoribbon were calculated in a supercell approach with Gamma-point sampling of the Brillouin zone. For the monolayer, a 19.12 x 19.12 Å unit cell was used, which corresponds to a 6 x 6 supercell of primitive WS_2 unit cell. A 16 Å vacuum region was introduced between the monolayers. For the nanoribbon, a 29.11 x 19.12 Å unit cell was used. This significantly larger X-dimension of the unit cell was necessary to reduce the interaction between the nanoribbon edges in adjacent unit cells. The supercell size was fixed, and all internal coordinates of the systems were completely relaxed until the forces on atoms were less than 0.04 eV/Å.

References

(1) P. Giannozzi, S. Baroni, N. Bonini, M. Calandra, R. Car, *et al*., QUANTUM ESPRESSO : a modular and open-source software project for quantum simulations of materials *J.Phys.:Condens.Matter*, **2009**, 21, 395502

(2) A. Molina-Sánchez and L. Wirtz, Phonons in single-layer and few-layer MoS2 and WS2 *Phys. Rev. B* **2011***,* 84, 155413

(3) W.J.Schutte,.J.L.De Boer, F.Jellinek, Crystal structures of tungsten disulfide and diselenide, *J. Solid State Chem.* **1987**, 70, 207

(4) P. Blaha, K. Schwarz, G. Madsen, D. Kvasnicka and J. Luitz, *WIEN2k*, An Augmented Plane Wave + Local Orbitals Program for Calculating Crystal Properties (Karlheinz Schwarz, Techn. Universität Wien, Austria), 2001. ISBN 3-9501031-1-2